A New Enhanced-Phase-Shift Modulation Strategy of Semi-Dual-Active-Bridge Converter for EV Application

Duy-Dinh NGUYEN, Goro FUJITA
Power System Laboratory
Shibaura Institute of Technology, Japan
Email: na14503@shibaura-it.ac.jp

Minh C. TA
Center for Technology Innovation
Hanoi Univ. of Science and Technology, Vietnam
Email: minh.tacao@hust.edu.vn

Abstract

This paper proposes a new modulation strategy for a bidirectional converter which is used to connect two ultra-capacitors and a traction battery in a hybrid energy storage system of an electric vehicle. Since the voltage across the ultra-capacitors varies in a very wide range, the isolated-semi-dual-active-bridge will be investigated instead of the non-isolated version. In order to save more energy, the system efficiency is enhanced by depressing the circulating current with the converter. This is done in this paper in a direct manner by estimating the load angle between the current and output voltage of one inverter then modifying the modulation parameters. A new technique based on second-order-generalized-integrator is develop to estimate such angle. Simulation study on a 10 kW converter shows that the system efficiency is enhanced about 9% in the forward and 7.4% in backward power transmission respectively by using the proposed modulation strategy instead of the conventional one.

Keywords: Isolated-dual-active-bridge, bidirectional converter, circulating current elimination, soft-switching, enhanced-phase-shift, single-phase-shift

1. Introduction

In recent years, application of Ultra Capacitor (UC) in the energy storage system (ESS) of Electric Vehicle EV) has been gained more attractions because of its fast charge and discharge characteristic. An UC can supports the EV in acceleration by shorten the speed-up time. During deceleration period, UC can help storing the regenerative energy from the traction motor. Using an UC alongside the conventional battery can prolong the lifetime of the battery itself.

Aiming to interface between the UC and the battery, a bidirectional DC/DC converter should be employed. For example, a non-isolated synchronous boost converter is a good option. However, while the battery voltage is almost constant, the UC voltage varies in a very wide range, from zero to the rated one. In order to obtain soft-switching, the inductance of the boost inductor should be relatively low. As a consequent, the inductor will have to sustain a high current ripple, and therefore, high AC loss. Furthermore, in spite of very high capacitance, the rated voltage of UC is relatively low. Connecting several UC banks in series can solve the low voltage problem, but balancing system must be used to protect the UC from over voltage failure.

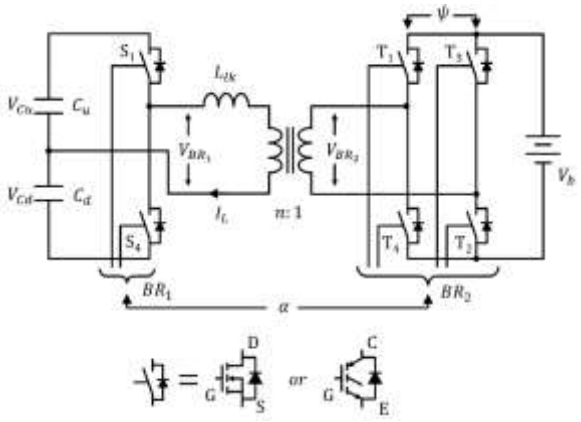

Fig. 1. Isolated-dual-active-bridge converter.

In order to deal with the high voltage ratio, an isolated bidirectional DC/DC converter, or so-called Dual-Active-Bridge (DAB) converter, can be considered instead of the non-isolated one. DAB topology is first introduced by De Doncker [2] in 1991. This kind of converter has many advantages over other topologies, such as, bidirectional power transmission, galvanic isolation, high voltage ratio, space saving because the leakage inductance of the transformer can be utilized as the power transmission container. Moreover, soft switching characteristics can be attained for all power electronic devices, that lead to high efficiency and high power density [3].

Fig. 1 illustrates a Semi-DAB (SDAB) converter which is intended to be applied for a hybrid energy storage system of an EV. A couple of UCs are connected in series. The primary winding of an isolated transformer with the ratio of n : 1 connects to the middle points of the UC branch and the half-bridge switching network BR_1. The total leakage inductance L_{lk} plays as the energy container. The secondary side of the transformer ties to the output of the H-bridge converter BR_2. The traction battery of the EV locates at the input of the H-bridge.

Conventionally, the power flow within the DAB converter is manipulated by the single phase shift (SPS) modulation [2], [4]–[9]. Obviously, it can also be used for SDAB converter. In the SPS method, all power electronic devices switch with the duty cycle of

50%. In the inverter BR_2, one leg is 180 degree phase shifted from each other. Another phase shift angle, named α, between the modulation of the two inverters is utilized to handle the power flow. Since the realization is very simple as well as the ability of zero voltage transition for all power electronic devices in a wide operation range, SPS scheme is widely used for DAB converter family. Nevertheless, due to only single phase shift is employed to control the system, some circulating current will occur at both inverters when transfer the power between the two sides. When the amplitude of the voltages are almost the same, this circulating current is insignificant and it only contributes to the soft-switching activities of switching devices. When the voltages are not matched, this current element is considerable that leads to the growth of the conduction loss and the copper loss. Appearance power on the high frequency transformer also increases. Additionally, soft-switching cannot be achieved in the whole operation range in this situation. Hence, a higher rating of power electronic components, and bigger size of magnetic devices may be required.

Several techniques based on advancing the commutation strategy have been proposed in order to reduce this reactive power and/or to extend the soft-switching region of a DAB converter. By adding one or two more degrees of freedom into the modulation, enhanced phase shift (EPS), dual phase shift (DPS), or triple phase shift (TPS) schemes can be realized. The EPS [10]–[12] scheme is almost the same as SPS, but in one of the two inverters, two legs are phase shifted in order to vary the duty cycle of the output AC voltage of the corresponding inverter to be smaller than 50%. Thanks to this inner phase shift, the voltage ratio between the two ends of the transmission inductor can be modified to help matching the voltage amplitude. In the DPS scheme [13]–[17], the inner phase shift is applied for both inverters with the same angle. Thus, the voltage ratio is kept constant but the root-mean-square values of the output voltages are changed to regulate the power flow. In TPS strategy [18]–[22], the inner phase shifts of the two inverters are different, so that both the ratio and the root-mean-square value of the voltages can be controlled. However, DPS and TPS are applicable only for the converters that have two H-bridge networks. For the SDAB one, only EPS scheme is considerable.

In this paper, a new modulation method based on EPS scheme will be examined. This method is intended to be applied for a SDAB converter depicted in Fig. 1. The operation principle of the converter modulated by EPS will be described in section II. The control target is to minimize the circulating current at one inverter of the twos and to achieve soft-switching for all power electronic devices. Note that, this circulating current exists due to the difference in phase between the current and the voltage responses. Thus, in section III, a new technique used to estimate this phase difference will be developed. After that, the compensated method for the phase difference will be introduced in section IV. As a result, all switching devices at the half-bridge network obtain both zero voltage and zero current commutation characteristics; meanwhile, all transistors belonging to the full-bridge network achieve zero voltage transition condition. Simulation results in section V will confirm the validity of the proposed modulation method.

2. Operation principle

For simpler analysis, the following assumptions are made:

- the transformer does not saturate,
- the transition time is so short that can be ignored,
- the voltage drop on power electronic components is neglected,
- the voltages across the UCs are equal.

Fig. 2 demonstrates the current and voltage waveforms of the SDAB converter in the forward power transmission mode, from the UCs to the battery. In the figure, U_{GS} is the triggering voltage of power electronic devices $S_{1,4}$ and T_{1-4} ; V_{br1} and V_{br2} are the output voltage of the half-bridge and full-bridge switching network, respectively; and I_L is the transferred current. Let the phase of the half-bridge switching network $S_1 - S_4$ be zero. The leg $T_1 - T_4$ is shifted α radian from the leg $S_1 - S_4$, where α is the outer phase shift angle; meanwhile, the leg $T_3 - T_2$ is shifted $\pi - \psi$ radian from the leg $T_1 - T_4$, where ψ is so-called the inner phase shift angle. The outer phase shift α is utilized to manipulate the power flow within the system. If α is positive, the power flows in a forward direction from the UCs to the battery and vice versa, if α is negative, the power is transferred in the

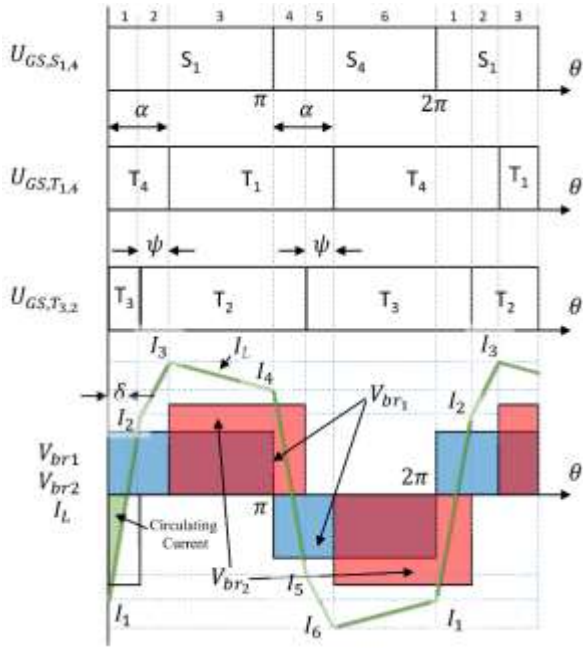

Fig. 2. Switching waveform of SDAB converter.

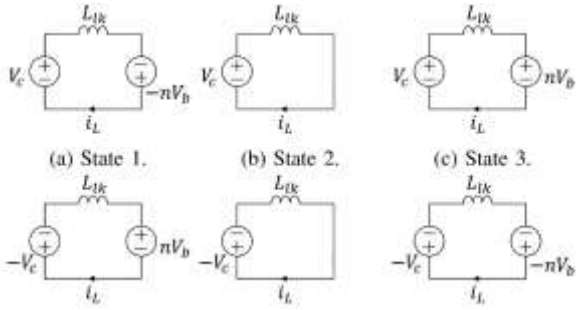

Fig. 3. Six switching states.

backward direction from the battery to the UCs. Concurrently, the inner phase shift ψ is employed to tune the switching pattern for better modulating performance.

Depending on the alignment of V_{br1} and V_{br2}, the operation can be divided by six switching states. For example, the modulation when $0 < \psi < \alpha$ depicted in the Fig. 2 can be classified as followed. Fig. 3 describes the primary referred equivalent circuit of each state.

- State 1: S_1 ON, T_{4-3} ON; S_4 OFF, T_{1-2} OFF

Let I_1 and I_2 be the current at the beginning and the end of this interval, respectively. The equivalent circuit of this state is indicated in the Fig. 3a. Ignore the internal resistance of the inductor, the relationship of I_1 and I_2 can be written as:

$$I_2 = I_1 + \frac{V_c + nV_b}{\omega_s L_{lk}} \times (\alpha - \psi) \quad (1)$$

where V_c and V_b are the voltage across the UCs and the battery, respectively; n is the transformer ratio; and ω_s is the switching frequency in radian.

- State 2: S_1 ON, T_{4-2} ON; S_4 OFF, T_{1-3} OFF

Since T_4 and T_2 are ON simultaneously, the secondary winding of the transformer is short. Fig. 3b represents the equivalent circuit during this interval. The current I_3 at the end of the second state can be calculated as:

$$I_3 = I_2 + \frac{V_c}{\omega_s L_{lk}} \times \psi \quad (2)$$

- State 3: S_1 ON, T_{1-2} ON; S_4 OFF, T_{4-3} OFF

As depicted in the Fig. 3c, the forward battery voltage is applied at the secondary side of the transformer. Equation (3) shows the calculation of the current at the end of this period:

$$I_4 = I_3 + \frac{V_c - nV_b}{\omega_s L_{lk}} \times (\pi - \alpha) \quad (3)$$

During the next three states, the voltage across the primary side of the transformer is reversed since the winding connects to the downside capacitor. Using the same analyzing manner as the previous states, the currents at the end of each state are expressed by (4), (5), (6), respectively.

- State 4: S_4 ON, T_{1-2} ON; S_1 OFF, T_{4-3} OFF

$$I_5 = I_4 + \frac{-V_c - nV_b}{\omega_s L_{lk}} \times (\alpha - \psi) \quad (4)$$

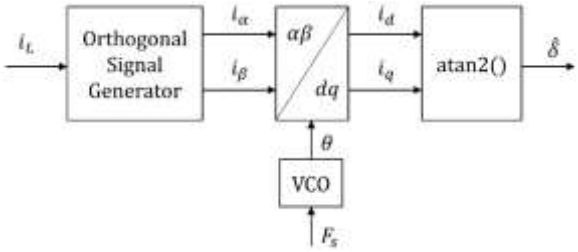

Fig. 4. Load angle estimator function block diagram.

- State 5: S_4 ON, T_{1-3} ON; S_1 OFF, T_{4-2} OFF

$$I_6 = I_5 + \frac{-V_c}{\omega_s L_{lk}} \times \psi \quad (5)$$

- State 6: S_4 ON, T_{4-3} ON; S_1 OFF, T_{1-2} OFF

$$I_1 = I_6 + \frac{-V_c + nV_b}{\omega_s L_{lk}} \times (\pi - \alpha) \quad (6)$$

Note that, at the steady state, $I_4 = -I_1$, $I_5 = -I_2$, and $I_6 = -I_3$. Substitute this constraints into (1), (2), and (3), the current at the state changing points can be computed by:

$$\begin{cases} I_1 = -\frac{V_c - nV_b}{2X_L} \times \pi - \frac{nV_b}{2X_L} \times 2\alpha + \frac{nV_b}{2X_L} \times \psi \\ I_2 = -\frac{V_c - nV_b}{2X_L} \times \pi + \frac{nV_b}{2X_L} \times 2\alpha - \frac{2V_c + nV_b}{2X_L} \\ I_3 = -\frac{V_c - nV_b}{2X_L} \times \pi - \frac{nV_b}{2X_L} \times 2\alpha - \frac{nV_b}{2X_L} \times \psi \end{cases} \quad (7)$$

where X_L is the reactance of total leakage inductor, which can be determined by $X_L = \omega_s L_{lk}$.

From (7) and Fig. 2, the load angle δ between the current I_L and the primary voltage V_{br1} can be approximated by (8) and (9):

$$\delta = \frac{-I_1}{I_2 - I_1} \times (\alpha - \psi) \quad (8)$$

$$= \frac{2\alpha - \psi + (M-1)\pi}{M+1} \quad (9)$$

where M is the voltage ratio, $\boldsymbol{M = \frac{V_1}{nV_2}}$.

Because of the load angle δ, there will be some current not transfer to the other side of the converter but only circulates within the inverter. When $\delta < 0$, the current is advanced over the voltage, leading to the hard-switching behavior of the switching devices. If the $\delta > 0$, this circulating current will force the voltage across the device to be zero before turning on. However, as mentioned earlier, a big value δ means high current stress, more appearance power on the high frequency transformer, high conduction and copper loss. From (9), as the inner phase shift angle ψ increases, the load angle δ decreases. The ideal case happens when:

$$\delta = 0 \leftrightarrow \psi = \frac{2\alpha}{(M-1)\pi}$$

Consequently, S_1 and S_4 turn on at zero voltage (ZVS) and turn off at zero current (ZCS) conditions.

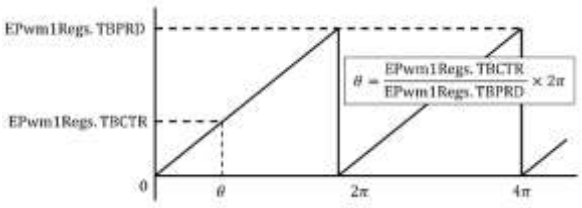

Fig. 5. Calculation of $\boldsymbol{\theta}$ in experiment.

For soft-switching of all power electronic devices, the following constrain must be satisfy:

$$\begin{cases} I_1 \le 0 \\ I_2 \ge 0 \\ I_3 \ge 0 \end{cases} \quad (10)$$

Solve (10) for α and ψ, the soft-switching condition can be rewritten as (11), whereas, the condition $M \le 1$ can be achieved easily by designing the transformer. In other words, if S_1 and S_4 are soft-switched, all power electronic components in the converter are also soft-switched.

$$\begin{cases} 0 < \psi < \alpha \\ M \le 1 \\ \delta \ge 0 \end{cases} \quad (11)$$

Note that, the six switching states may be varied when α and ψ changed. As a result, the approximation of δ according to (9) and the soft-switching constrain are only valid for the case $0 < \psi < \alpha$, and may be not valid for other circumstances. Nevertheless, analyzing all operation modes of a SDAB converter is out of the scope of this paper. Instead, this paper proposes a new method to estimate the load angle δ regardless the operation modes, and focuses on how to eliminate this load angle to enhance the switching performance of the converter.

3. Estimation of the load angle

The estimation method is as followed: firstly, an orthogonal signal will be generated from the measured current; after that, a Park transformation is utilized to yield the direct and the quadrature components of the transferred current; finally, the estimated load angle $\hat{\delta}$ is the arctangent of the ratio of the quadrature and the direct current. The function block diagram of the estimator is depicted in the Fig. 4. The two current signal i_α and i_β are generated from the Orthogonal Signal Generator. One signal, says i_α , should be the same in phase with the original one i_L; meanwhile i_β should be 90 electrical degree shifted from i_α. The synchronous signal θ is provided by a Voltage-Control-Oscillator (VCO) function block. F_s is the switching frequency in Hertz. In order to avoid the division-by-zero problem, the atan2() function will be employed to calculate $\hat{\delta}$, which is the estimated value of the load angle δ. The estimator model expressed in Fig. 4 is intended for simulation. In experiment, θ can be easily calculated from the pulse-width-modulation (PWM) system of the micro-processor by dividing the PWM counter over the PWM period then multiplying by 2π.

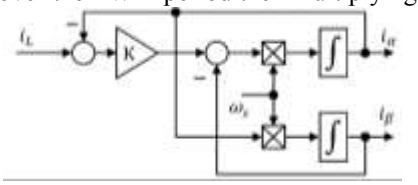

Fig. 6. Second-order generalized integrator function block diagram.

Fig. 5 demonstrates the calculation of θ using digital signal processor TMS320F28335 manufactured by Texas Instrument Incorporation.

Regarding the orthogonal signal generator, there are several possible techniques in literatures such as Hilbert transformation [23], Kalman filter [24], all-pass filter (APF) [25], [26], or second-order generalized integrator (SOGI) [27]. Among them, those based on the Hilbert transformation and the Kalman filter are relatively complicated and consume high computational resources; APF is simple and easy to be realized, however, it is only suitable for pure sinusoidal signals; SOGI based scheme not only generates the orthogonal signal but also filters out the harmonics from the original one without transportation delay. Furthermore, SOGI can also be used as a phase-lock-loop system. Thanks to SOGI, the output signal i_α and i_β will be pure sinusoidal, that can make the estimator more accurate. As depicted in Fig. 2, the waveform of the transferred current is AC multiform polygonal depending on the operation modes. Thus, SOGI is most appropriate, then it will be selected in this paper as the orthogonal signal generator.

The function block of SOGI is illustrated in Fig. 6, where ω_s is the switching frequency in radian; K is the gain ratio, in this paper, K is set to 0.3 for better harmonics rejection [27]; i_L is the measured current; and i_α and i_β are the two outputs of SOGI. The transfer functions from i_L to i_α and from i_L to i_β are given by (12) and (13), respectively:

$$H_\alpha(s) = \frac{i_\alpha(s)}{i_L(s)} = \frac{K\omega_s s}{s^2 + K\omega_s s + \omega_s^2} \quad (12)$$

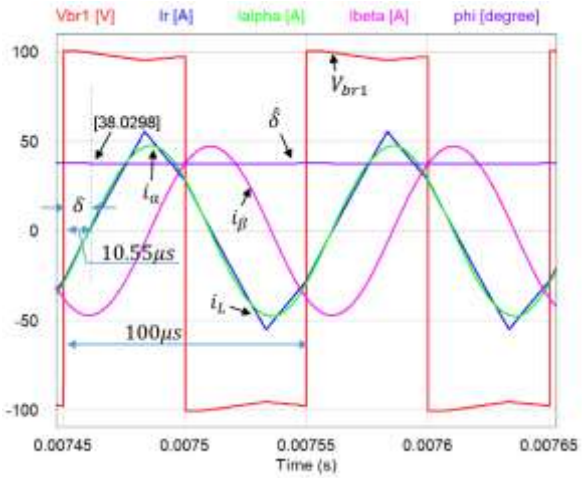

Fig. 7. Transformed current waveforms.

$$H_\beta(s) = \frac{i_\beta(s)}{i_L(s)} = \frac{K\omega_s^2}{s^2 + K\omega_s s + \omega_s^2} \qquad (13)$$

where s is the Laplace operator.

The performance of SOGI is illustrated in Fig. 7. In this illustration, the switching frequency is 10 kHz, then each switching period lasts for 100µs. As can be seen, the current lags after the voltage 10.55 µs, thus the simulated load angle is:

$$\delta = \frac{10.55}{100} \times 360^o = 37.98^o$$

meanwhile the estimated one, $\hat{\delta}$, is 38.03° at the same instance. The angle error is about −0.13%, so small that can be ignored.

4. Circulating current compensation strategy

As noted before, when the inner phase shift angle ψ increases, the load angle δ decreases, then help reducing the circulating current. Furthermore, if the load angle is zero, δ = 0, the circulating current is eliminated, then S_1 and S_4 achieve both ZVS and ZCS meanwhile $T_1 - T_4$ obtain ZVS characteristics. This can be accomplished by using the compensation strategy described in Fig. 8.

The original idea is to compensate the load angle by accumulating the estimated one $\hat{\delta}$ into the inner phase shift angle ψ. As long as $\hat{\delta}$ is other than zero, ψ increases or decreases to force it to zero. For example, if $\hat{\delta}$ is positive, then S_1 and S_4 are ZVS. However, due to the circulating current exists on the half-bridge switching network, it should be minimized. Since $\hat{\delta} > 0$, the integrator INT in the compensator indicated in the Fig. 8 accumulates. The time constant of INT is set to be one switching period (i.e. $1/F_s$). Hence, ψ increases leading to the decrement of $\hat{\delta}$. When $\hat{\delta}$ is completely eliminated, $\hat{\delta} = 0$, ψ stops increasing and remains constant. As a consequence, S_1 and S_4 achieve both ZVS and ZCS meanwhile T_{1-4} attain ZVS as analyzed in section II. Conversely, when $\hat{\delta}$ is negative, S_1 and S_4 is hard switching, then ψ should reduce to raise $\hat{\delta}$. The integrator INT helps doing this by accumulating the negative value of $\hat{\delta}$. Since the time constant of INT is $1/F_s$, $\hat{\delta}$ will be expelled after few switching cycles.

From another respect, $\hat{\delta}$ estimated by SOGI is not the actual load angle but the approximated one since the transferred current waveform is not pure sinusoidal. Hence, some angle error may exist leading to the continuously increment of ψ even in the steady state. The limiter LMT is then utilize accompanying with an anti-windup mechanism to keep ψ in range. The limitation of ψ setting in this paper is $\left[-\frac{\pi}{2}, \frac{\pi}{2}\right]$ because a wider value of ψ may restrict the maximum power transmission capability of the converter, but a narrower one will limit the circulating current rejection ability.

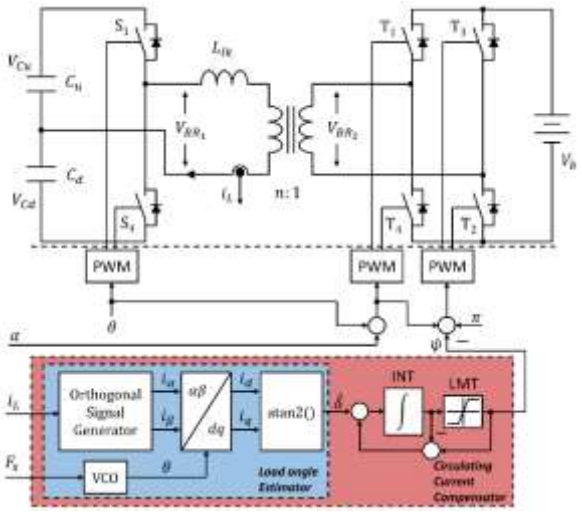

Fig. 8. Compensation strategy diagram.

Obviously, applying the proposed compensation method will affect the amplitude of the power flow. For a given outer phase shift angle α, a bigger value of ψ means a smaller transferred power and vice versa. Therefore, when ψ is being manipulated to avoid the circulating current, α should be changed to regulate the power amplitude concurrently. This can be done automatically by employing a close current control loop, in which i_L is the controlled output, and α is the
control variable. Then, the current controller is designed with an appropriate margin to compensate for the variation of the power amplitude when ψ changes. Nevertheless, designing such a controller is out of the scope of this paper and it will be discussed in the future studies.

5. Simulation results

In order to evaluate the performance of the proposed modulation method, the simulation is conducted in comparison with the conventional single phase shift (SPS) control scheme. The parameters of the investigated system is listed in Table I. The switching frequency are the same at 10 kHz. In both modulation methods, the power from 1 kW to 10 kW will be transferred in bidirectional ways. Because both two sides of the converter are DC voltage sources, the delivered and received powers can be calculated without difficulty. The system efficiency obtained from simulation is the ratio between the received power over the delivered one. By applying this calculation method, all power dissipation including copper loss, conduction loss, switching loss, etc. are regarded. Fig. 9a and Fig. 9b demonstrate the performance comparison of the two control methods in both transmission modes.

Comparing the simulated efficiency, at the light load condition, the proposed control method shows a much

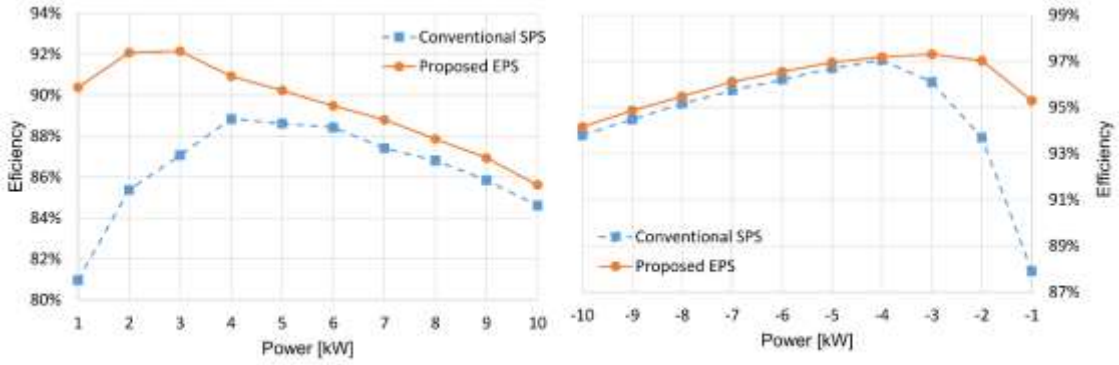

(a) Forward mode. (b) Backward mode.

Fig. 9. Performance comparison.

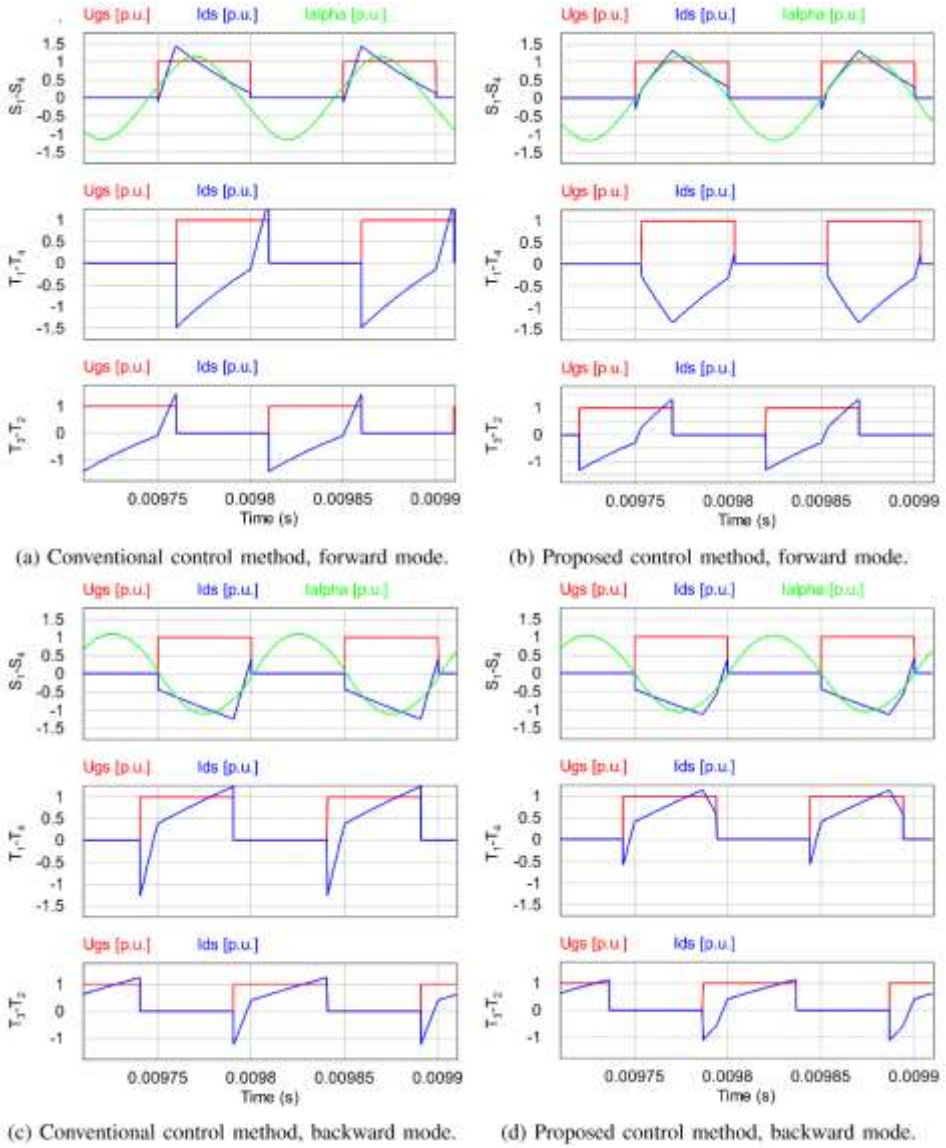

(a) Conventional control method, forward mode. (b) Proposed control method, forward mode.

(c) Conventional control method, backward mode. (d) Proposed control method, backward mode.

Fig. 10. Switching behavior of power electronic devices at the rated load condition.

better performance than the conventional one. The efficiency is boosted from 80.96% to 90.38% at 1 kW forward power transmission. The reversed path with the same power amount also records an enhancement of 7.39% in efficiency, from 87.90% to 95.29%. At the middle and rated load condition, the efficiency gaps decreases, however, the new modulation strategy is still the superior in both power transmission ways. In order to evaluate the switching behavior of the power electronic devices in the system, the rated

power of 10kW is transferred in bidirectional ways using the two control methods. Fig. 10 illustrates the current and the triggering waveforms of two switching-devices of each inverter in all operation modes. As shown in Fig. 10b and Fig. 10d, there is no phase difference between the α component of the transferred current and the output voltage of the half-bridge inverter in the forward mode. In the backward mode, the phase difference is exactly $-\pi$ for reverse power to flow. In all cases, all switching devices achieve ZVS condition. Since the current waveform is not pure sinusoidal, S_1 and S_4 do not obtain ZCS but only low current turn off characteristics. Furthermore, comparing to the current response using conventional SPS modulation method illustrated in Fig. 10a and Fig. 10c, the peak current when applying the new EPS scheme is lower. Thus, the current stressing on the power electronic devices is attenuated.

Furthermore, by utilizing the proposed EPS modulation technique, the current shape is relatively closer to the sinusoidal waveform. Therefore, the power dissipation because of high frequency harmonics will reduce. This also contribute to the efficiency enhancement of the new modulation strategy.

6. Conclusion

This paper proposes a new modulation strategy for an isolated-semi-dual-active-bridge converter intending to apply in hybrid energy storage system of electric vehicles. The converter is utilized to bidirectional power transmit between a couple of ultra-capacitor and the traction battery of the EV. The new method estimates the load angle, which is the cause of circulating current, then try to depress it. The estimator is based on a second-order-generalized-integrator and Park transformation, which can be programmed on a digital controller without difficulty. The simulation result has shown that, the new modulation technique can save more energy than the conventional one since the system efficiency is improved, especially at the light load condition.

References

[1] R. Carter , A. Cruden and P. J. Hall "*Optimizing for efficiency or battery life in a battery/super-capacitor electric vehicle*", IEEE Trans. Veh. Technol., vol. 61, no. 4, pp.1526 -1533 2012

[2] De Doncker. R. W. A. A., Divan. D. M., Kheraluwala. M. H., "*A three-phase soft-switched high-power-density DC/DC converter for high-power applications*," IEEE Transaction on Industry Applications, vol.27, no.1, pp.63,73, Jan/Feb 1991

[3] F. Krismer , J. Biela and J. W. Kolar, "*A comparative evaluation of isolated bi-directional DC/DC converters with wide input and output voltage range*", Proc. IEEE Ind. Appl. Conf., pp.599-606 Oct. 2005

[4] M. H. Kheraluwala, R. W. Gascoigne, D. M. Divan, and E. D. Baumann, "*Performance characteriza-tion of a high-power dual active bridge dc-to-dc converter*," IEEE Trans. Ind. Appl., vol. 28, no. 6, pp. 1294-1301, Nov./Dec. 1992.

[5] Xiaodong Li, Bhat. A. K. S., "*Analysis and Design of High-Frequency Isolated Dual-Bridge Series Resonant DC/DC Converter*," IEEE Trans. Power Electron. vol.25, no.4, pp.850-862, April 2010

[6] S. Inoue and H. Akagi, "*A bidirectional dc-dc converter for an energy storage system with galvanic isolation*," IEEE Trans. Power Electron., vol. 22, no. 6, pp. 22992306, Nov. 2007.

[7] C. Mi,H. Bai, C.Wang, and S.Gargies, "*Operation, design and control of dual H-bridge-based isolated bidirectional dc-dc converter*," IET Power Electron., vol. 1, no. 4, pp. 507-517, Apr. 2008.

[8] D. Costinett, D. Maksimovic, and R. Zane, "*Design and control for high efficiency in high step-down dual active bridge converters operating at high switching frequency*," IEEE Trans. Power Electron., vol. 28, no. 8, pp. 3931-3940, Aug. 2013.

[9] Biao Zhao, Qiang Song, Wenhua Liu, and Yandong Sun, "*Overview of Dual-Active-Bridge Isolated Bidirectional DCDC Converter for High-Frequency-Link Power-Conversion System*," IEEE Trans. on Power Electronics, vol.29, no.8, pp.4091,4106, Aug. 2014.

[10] Oggier, G.G.; Garcia, G.O.; Oliva, A.R., "*Switching Control Strategy to Minimize Dual Active Bridge Converter Losses*," IEEE Trans. Power Electron. vol.24, no.7, pp.1826-1838, July 2009

[11] G. G. Oggier, G. O. Garcia, and A. R. Oliva, "*Modulation strategy to operate the dual active bridge dc-dc converter under soft switching in the whole operating range*," IEEE Trans. Power Electron., vol. 26, no.4, pp. 1228-1236, Apr. 2011.

[12] G. G. Oggier, R. Ledhold, G. O. Garcia, A. R. Oliva, J. C. Balda, and F. Barlow, "*Extending the ZVS operating range of dual active bridge highpower dc-dc converters,*" in Proc. IEEE Power Electron. Spec. Conf., 2006, pp. 1-7.

[13] Hua Bai, Mi. C., "*Eliminate Reactive Power and Increase System Efficiency of Isolated Bidirectional Dual-Active-Bridge DCDC Converters Using Novel Dual-Phase-Shift Control,*" IEEE Trans. Power Electron. vol.23, no.6, pp.2905,2914, Nov. 2008

[14] H. Bai, Z. Nie, and C. Mi, "*Experimental comparision of traditional phase-shift, dual-phase-shift, and model-based control of isolated bi-directional dc-dc converters*," IEEE Trans. Power Electron., vol. 25, no. 6, pp. 1444-1449, Jun. 2010.

[15] B. Zhao, Q. Song, and W. Liu, "*Power characterization of isolated bidirectional dual-*

active-bridge dc-dc converter with dual-phase-shift control," IEEE Trans. Power Electron., vol. 27, no. 9, pp. 4172-4176, Sep. 2012.

[16] B. Zhao,Q. Song,W. Liu, and W. Sun, "*Current-stress-optimized switching strategy of isolated bidirectional dc-dc converter with dual- phase-shift control,*" IEEE Trans. Ind. Electron., vol. 60, no. 10, pp. 4458-4467, Oct. 2013.

[17] B. Zhao, Q. Song, and W. Liu, "*Efficiency characterization and optimization of isolated bidirectional dc-dc converter based on dual-phase-shift control for dc distribution application*," IEEE Trans. Power Electron.,vol. 28, no. 4, pp. 1711-1727, Apr. 2013.

[18] F. Krismer and J. W. Kolar, "*Efficiency-optimized high-current dual active bridge converter for automotive applications*," IEEE Trans. Ind. Electron., vol. 59, no. 7, pp. 2745-2760, Jul. 2012.

[19] F. Krismer and J. W. Kolar, "*Closed form solution for minimum conduction loss modulation of DAB converters",* IEEE Trans. Power Electron., vol. 27, no. 1, pp. 174-188, Jan. 2012.

[20] K. Wu, C. W. Silva, and W. G. Dunford, "*Stability analysis of isolated bidirectional dual active full-bridge dc-dc converter with triple phase shift control",* IEEE Trans. Power Electron., vol. 27, no. 4, pp. 2007-2017, Apr. 2012.

[21] F. Krismer, and J. W. Kolar "*Accurate small-signal model for the digital control of an automotive bidirectional dual active bridge*", IEEE Trans. Power Electron., vol. 24, no. 12, pp.2756-2768, 2009

[22] A. K. Jain and R. Ayyanar, "*PWM control of dual active bridge: Comprehensive analysis and experimental verification*," IEEE Trans. Power Electron., vol. 26, no. 4, pp. 1215-1227, Apr. 2011.

[23] M. Saitou and T. Shimizu, "*Generalized theory of instantaneous active and reactive powers in single-phase circuits based on Hilbert transform*," in Proc. 33rd Annu. IEEE PESC, Jun. 2002, pp. 1419-1424.

[24] K. De Brabandere, T. Loix, K. Engelen, B. Bolsens, J. Van den Keybus, J. Driesen, and R. Belmans, "*Design and operation of a phase-locked loop with Kalman estimator-based lter for single-phase applications*," in Proc. IEEE Ind. Electron. Soc. Conf., 2006, pp. 525-530.

[25] R. Y. Kim, S. Y. Choi, and I. Y. Suh, "*Instantaneous control of average power for grid tie inverter using single phase D-Q rotating frame with all pass filter*," in Proc. IEEE Annu. Conf. Ind. Electron. Soc., Nov. 2004, pp. 274-279

[26] Mohammad Monfared, Saeed Golestan, and Josep M. GuetTero, "*Analysis, Design, and Experimental Verification of A Synchronous Reference Frame Voltage Control for Single-Phase Inverters*," IEEE Trans. On Industrial Electronics, vol. 61, no. 1, pp. 258-269, Jan 2014.

[27] M. Ciobotaru, R. Teodorescu, and F. Blaabjerg, "*A new single-phase PLL structure based on second order generalized integrator*," in Proc. 37th IEEE PESC, Jun. 2006, pp. 1-6

NGUYEN Duy Dinh received the B.E., and M.Sc. degrees in school of electrical engineering, Hanoi University of Science and Technology (HUST), Vietnam, in 2009 and 2012, respectively. Beside working as a lecturer at the Dept. of Industrial Automation of HUST, he took part in the Centre for Technology Innovation, HUST as a researcher. He has been a PhD student in Shibaura Institute of Technology, Tokyo, Japan since 2014. His research interests are Design and Control of Power electronic converter, and its application on Power system, Electric Vehicle and Renewable Energy Storage System.

GORO FUJITA (S'96–A'97–M'02) received the B.E., M.E., and Ph.D. degrees in electrical engineering from Hosei University, Tokyo, Japan, in 1992, 1994, and 1997, respectively. He was a Research Student with Tokyo Metropolitan University, Tokyo, Japan, in 1997. He is currently a Professor with the Shibaura Institute of Technology, Tokyo, Japan. He is a First Class Licensed Engineer in Japan. His current research interests include power system control, including dispersed power systems.

Ta Cao Minh graduated from Czech Republic in 1986 and got Ph.D. at Laval University, Canada 1997. He had 6 years working in industrial and academic environments in Japan (1998 – 2004) and visiting professor in Taiwan (2010), Australia (2012) and France (2015). He became Assoc. Prof. in the Department of Industrial Automation, HUST in 2009. Besides, he is the Director of Center for Technology Innovation, HUST. His research interest is focused on Control of Electric Drive, Power Electronics, applications for electric vehicles and renewable energy. Being the author of 27 papers published in international journals and proceedings, 14 Japanese granted patents, Assoc. Prof. Minh was awarded the 2nd Prize for best paper of the IEEE-IAS Conference in 2000 and the C Prize for the inventions in NSK Co. (Japan) in 2012. He was the IEEE Vietnam Section Chair (2008 – 2011) and presently the General Secretary of the Vietnam Automation Association (2014 – 2019).